Pergamon

Acta Materialia 50 (2002) 1405–1420

Acta MATERIALIA

www.actamat-journals.com

# Molecular dynamics simulation of triple junction migration

M. Upmanyu [a, b], D.J. Srolovitz [1a, b, c,*], L.S. Shvindlerman [d, e], G. Gottstein [e]

[a] *Princeton Materials Institute, Princeton University, Princeton, New Jersey, NJ 08540, USA*
[b] *Department of Mechanical and Aerospace Engineering, Princeton University, Princeton, NJ 08540, USA*
[c] *Department of Materials Science and Engineering, University of Michigan, Ann Arbor, MI 48109-2136, USA*
[d] *Institut für Metallkunde und Metallphysik, RWTH Aachen, D-52056 Aachen, Germany*
[e] *Institute of Solid State Physics, Russian Academy of Sciences, Chernogolovka, Moscow distr. 142432, Russia*

Received 18 June 2001; received in revised form 3 December 2001; accepted 5 December 2001

**Abstract**

We present a molecular dynamics simulation study of the migration of grain boundaries with triple junctions. We have monitored the grain boundary profile, triple junction angles and rate of grain boundary migration with and without triple junctions as a function of grain size, grain misorientation, direction of migration and temperature in a series of configurations designed to ensure steady-state migration. The present results demonstrate that triple junction mobility is finite and can be sufficiently small to limit the rate of grain boundary migration. The drag on grain boundaries due to limited triple junction mobility is important at small grain sizes, low temperature and near high symmetry grain misorientations. This drag limits the rate of grain boundary migration and leads to triple junction angles that differ substantially from their equilibrium value. Simulation data suggest that triple junction drag is much more a factor at low temperature than at high temperature. The triple junction mobility is shown to depend upon the direction of triple junction migration. The present results are in excellent qualitative agreement with experimental observations. 

*Keywords:* Molecular dynamics; Grain boundary migration; Triple junctions

## 1. Introduction

Triple junctions are linear defects along which three grain boundaries meet. They exhibit thermodynamic properties unique from those of their constituent grain boundaries. Triple junctions can act as short circuit diffusion paths [1,2], serve as preferential sites for the nucleation of new phases, cavities, cracks [3] and corrosion [4], play an important role in plastic deformation [5], etc. Recent research has focused on the link between these unique properties and the thermodynamic and atomic structure of triple junctions. It is convenient to think of triple junctions in terms of a cylindrical core [6], with only a localized displacement field, quite analogous to that of a dislocation [7,8]. King et al. [9] have performed a detailed study of the structure of symmetrical triple junctions. The unrelaxed atomic structure of these junc-

* Corresponding author. Tel.: +1-609-258-5138; fax: +1-609-258-5877.
*E-mail address:* srol@princeton.edu (D.J. Srolovitz).
[1] Present address: Computer Science and Mathematics Division, Oak Ridge National Laboratory, Oak Ridge, TN 37831-6359, USA.

1359-6454/02/$22.00 
PII: S1359-6454(01)00446-3

tions has also been investigated by superposition of three, rotated three-dimensional lattices [10] and by matching the two-dimensional structures of grain boundaries [11]. On the basis of atomistic simulations, Srinivasan et al. [12] reported the existence of negative triple junction energies, while Caro and Van Swygenhoven [13] reported positive triple junction energies. Thus, the properties of these defects are strongly related to their atomic-scale structure. It is expected, therefore, that triple junctions also possess unique structure-sensitive kinetic properties as well. In this paper, we examine the intrinsic mobilities of triple junctions and their influence on grain boundary migration via dynamic atomistic simulations.

In equilibrium three phase fluid systems, the angles at which the three two-phase interfaces meet can be described from the surface tensions of the constituent interfaces (i.e. the Young–Duprè angles). Similarly, the equilibrium dihedral angles along which three grain boundaries meet are determined by a balance of the surface (interface) tensions and torques [14]. It is these fixed dihedral angles that maintain the boundary curvature that control grain growth/shrinkage. In two dimensions, this gives rise to the well known rule for isotropic grain growth: a grain grows if $n>6$ and shrinks if $n<6$, where $n$ is the number of grain edges [15]. Classical theories of grain growth assume that dihedral angles remains fixed, at equilibrium values, during grain growth. This assumption is of questionable validity based upon recent experience with dihedral angles in (partially) fluid systems [16,17] as well as experiments on grain boundary triple junctions (see e.g. Ref. 18).

As the grain boundaries that meet at a triple junction migrate, a necessary and sufficient condition for the dihedral angles to remain fixed is that the intrinsic triple junction mobility $M_{tj}$ is infinite. This can be understood in terms of the motion of the constituent grain boundaries. Assuming that grain boundary motion is dissipative (and overdamped), the boundary velocity, $v_b$, and driving force, $F_b$, are related by Ref. 19

$$v_b = M_b F_b, \tag{1}$$

where $M_b$ is the boundary mobility. When the driving force is associated with boundary curvature $\kappa$ (as in grain growth), Eq. (1) can be rewritten as

$$v_b = M_b \gamma \kappa, \tag{2}$$

where $\gamma$ is the grain boundary energy. Since there is a singularity in the grain boundary curvature at the triple junction, Eq. (2) suggests that any deviations from the equilibrium dihedral angles are restored with infinite velocity. Therefore, triple junctions angles are rigorously fixed at their equilibrium values and represent boundary conditions on the relative slopes of the boundaries meeting at the junction. By analogy with the force–velocity relation for grain boundaries, it is reasonable to postulate that the triple junction velocity $v_{tj}$ is proportional to the driving force it experiences, $F_{tj}$

$$v_{tj} = M_{tj} F_{tj}. \tag{3}$$

Preservation of the equilibrium dihedral angles during boundary migration implies that $F_{tj}$ is identically zero. Finite triple junction mobility would then imply that the triple junction migration rate $v_{tj}$ must always be zero. The existence of a finite triple junction migration rate with equilibrium triple junction angles is possible only if the triple junction mobility is infinite.

The preceding analysis was based on continuum descriptions such that grain boundaries are sharp interfaces and triple junctions are mathematical lines. This neglects the inherently atomic nature of these defects. The finite velocity motion of such boundaries and triple junctions necessitates atomic rearrangements over finite distances and times. Since triple junctions have atomic structure distinct from those of their constituent boundaries, a distinct, finite, intrinsic triple junction mobility seems plausible. The apparent contradiction between this argument and those that led to the conclusion that triple junction mobilities are infinite raises several questions. Are dynamic triple junction angles different from equilibrium angles? If so, how large are the deviations? How large is the triple junction mobility and how does it compare with those of its constituent grain boundaries? How does the triple junction mobility depend on such factors as the relative orientations of the bounding grains,

temperature, velocity (i.e. is Eq. (3) valid with a constant $M_{tj}$), grain size and direction of triple junction motion? We address these issues here.

Theoretical analysis by Galina et al. [20] have shown that for deviation of the dynamic triple junction angles from their equilibrium static angles, the triple junctions migrate with a finite mobility which can impose a drag on boundary migration. The drag effect is sensitive to the extent of the deviation in the angles and can be quantified in terms of a dimensionless triple junction mobility parameter defined as $\Lambda = M_{ij}w/M_b$. Czubayko et al. [18] measured triple junction mobilities and angles and demonstrated that significant deviations from equilibrium angles do occur and that triple junction mobilities are finite. Unfortunately, in even the purest materials, impurity segregation to boundaries significantly modifies grain boundary mobilities and, hence, we expect this to also be the case for triple junction mobilities. Therefore, while these measurements provided the first quantitative data on non-equilibrium triple junctions, the intrinsic behavior of triple junctions remains open.

In this paper, we present results from molecular dynamics simulations designed to systematically examine the mobilities of triple junctions and their effects on grain boundary migration. This represents the first atomic scale study aimed at quantifying the effect of triple junctions on grain boundary kinetics. We first outline the theory upon which this study relies and describe the simulation procedure employed. We then report triple junction kinetics as a function of grain size $w$, boundary misorientation $\theta$, and temperature $T$ for two different triple junction geometries. The geometries are designed to force exactly the same triple junctions to migrate in opposite direction. We report dynamic and static dihedral angle measurements and triple junction mobilities for thirteen different sets of triple junctions. These triple junction data are analyzed in light of the mobilities of the constituent boundaries, measured in previous simulation studies [24,26]. Finally, the implications of the present results on the evolution of polycrystalline microstructures are discussed.

## 2. Theoretical background

The present study focuses on the determination of the intrinsic triple junction mobilities in simulations where the migration is driven by grain boundary curvature. Two simulation geometries designed to achieve steady-state boundary and triple junction migration and from which the steady-state triple junction mobility may be extracted are shown in Fig. 1. In the geometry of Figs. 1a and b, the boundary curvatures are such that the triple junction moves either into or away from grain $a$ (referred to as the + and − directions, respectively). Three grains $a$, $b_1$ and $b_2$ separated by three grain boundaries with misorientations $\theta_{ab_1}$, $\theta_{ab_2}$ and $\theta_{b_1b_2} = \theta_{ab_1} + \theta_{ab_2}$ meet at the triple junction (the simulation are performed in two dimensions). The $b_1b_2$ grain boundary is assumed to be symmetric such that $\theta_{ab_1} = -\theta_{ab_2}$ and the $ab_1$ and $ab_2$ boundaries are equivalent. The orientations of the constituent grains in the two geometries are chosen such that the triple junctions in Figs. 1a and b are structurally identical. The force balance associated with the grain boundary (surface) tensions (in the direction parallel to the $b_1$ $b_2$ boundary) at the triple junction results in a thermodynamic driving force, $F_{tj}$ given by,

$$F_{tj}^{\pm} = 2\gamma_{ab}\cos\beta_d^{\pm} - \gamma_{bb} = \mp 2\gamma_{ab}(\cos\beta_d^{\pm} - \cos\beta_s), \quad (4)$$

where the superscript ± indicates that the variable applies to either the '+' or '−' configuration, $\beta_d$ is one-half the dynamic included angle within grain, $a$ and $\gamma_{ab}$ and $\gamma_{bb}$ are the grain boundary energies (if the boundary energy depends on boundary inclination, then the boundary energies must be replaced with $\gamma_{\eta\psi} + \partial^2\gamma_{\eta\psi}/\partial\varphi^2$, where $\varphi$ refers to the orientation of the grain boundary normal and $\eta$ and $\psi$ represent either $a$ or $b$). In static equilibrium, the net force on the triple junction is zero, $F_{tj}$=0, such that the static value of $\beta$ is given by $2\gamma\cos\beta_s = \gamma_{bb}$, which is used in the second equality in Eq. (4) (where we write $\gamma_{ab}$=$\gamma$ for simplicity). Combining Eqs. (3) and (4) yields an expression for the triple junction migration rate: $v_{tj} = M_{tj}^{\pm}F_{tj} = \mp 2\gamma M_{tj}^{\pm}(\cos\beta_d^{\pm} - \cos\beta_s)$.

We can easily extract the triple junction migration rate in terms of a quantity which can be extracted from the simulations, i.e. the rate of

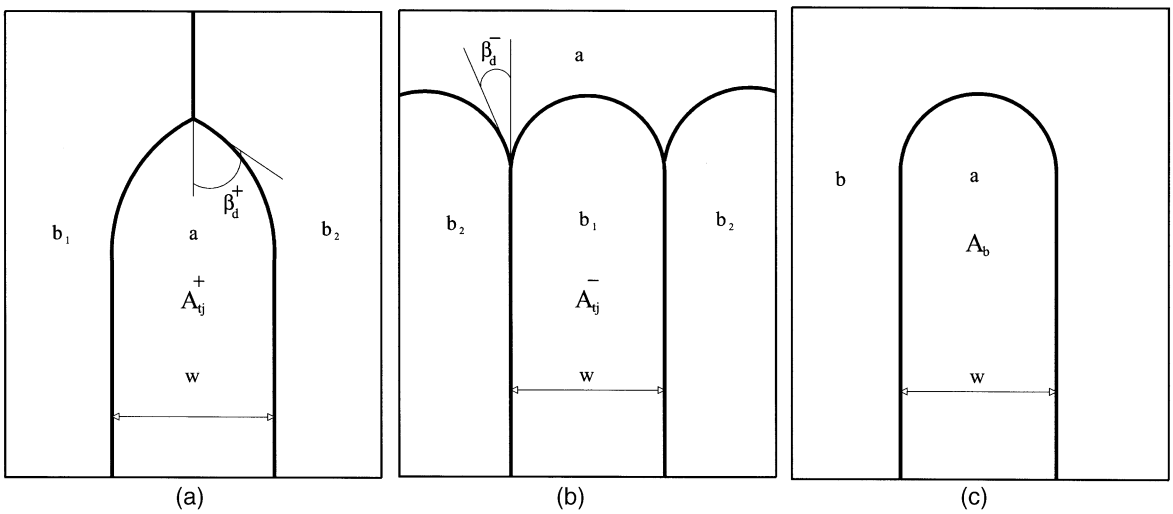


Fig. 1. Schematic illustrations of the geometries employed in the simulations. The definition of the triple junction angle $\beta$, half-loop grain width $w$ and grain identities are shown. The orientations of the $a$, $b_1$, and $b_2$ grains are the same in all three geometries. The misorientation across the $ab_1$ and the $ab_2$ boundaries is $\pm\theta$ and that across the $b_1b_2$ boundary is $2\theta$. The simulation geometries in a) and b), referred to as the '+' and '−' geometries because the $b_1b_2$ boundary increases or decreases, respectively, during curvature driven boundary migration. The geometry in c) represents the simulation cell used to study boundary migration in the absence of a triple junction and contains no $a$ boundary.

change of area $\dot{A}_{tj}^{\pm}$ of the half-loop grain (grain $a$ in Fig. 1a and grain $b$ in Fig. 1b). Geometrically, $\dot{A}_{tj}^{\pm}$ is simply the product of the width $w$ of the half-loop grain and the triple junction velocity, $v_{tj}$: $\dot{A}_{tj}^{\pm} = v_{tj}^{\pm} w = 2\gamma M_{tj}^{\pm} w|\cos\beta_d^{\pm} - \cos\beta_d|$. In the simulations, we measure $\dot{A}_{tj}^{\pm}$, $\beta_d^{\pm}$ and $\beta_s$ for each set of simulation conditions (simulations geometry, misorientation $\theta$, width $w$ and temperature $T$) and use the expression for $\dot{A}_{tj}^{\pm}$ to extract the reduced mobility of the triple junction. Galina et al. [21] and Gottstein et al. [22] analytically determined the shapes of the migrating grain boundaries and triple junctions in the geometries of Fig. 1 under the assumption of motion by mean curvature, inclination independent boundary energies (i.e. a spherical Wulff plot), and constant $\beta_d^{\pm}$ and showed

$$v_{tj}^{+} = \frac{2\beta_d^{+} M_b\gamma}{w};\ \dot{A}_{tj}^{+} = 2\beta_d^{+} M_b\gamma \tag{5a}$$

$$v_{tj}^{-} = \frac{-2[\ln(\sin\beta_d^{-})]M_b\gamma}{w};\ \dot{A}_{tj}^{-} = -2\ln(\sin\beta_d^{-})M_b\gamma \tag{5b}$$

where $M_b$ is the mobility of the $ab$ grain boundaries. Eqs. (5a) and (5b) can be used to analytically determine the triple junction angle in terms of the rate of change of grain area and the properties of the bounding grain boundaries (i.e., the reduced boundary mobility). The reduced mobility $M_b\gamma$ is extracted from bicrystal simulations in the geometry shown in Fig. 1c, where the velocity of the grain apex is [23] $v_b = \pi M_b\gamma/w$.

The ratio of the triple junction mobility to that of the constituent grain boundaries, under identical conditions can be used to quantify the effect of triple junctions on grain boundary migration: $\Lambda^{\pm} = M_{tj}^{\pm} w/M_b$. The width of the half-loop grain $w$ is included in the definition of $\Lambda^{\pm}$ because the triple junction and grain boundary mobilities (Eqs. (1) and (3)) have different dimensionalities. For $\Lambda^{\pm} \gg 1$, the triple junction mobility is large compared with the boundary mobility and, hence, the triple junction mobility provides little drag on the boundary motion. In this limit, the triple junction is in quasi-equilibrium and the triple junction angle should be approximately equal to the equilibrium angle (i.e., $\beta_d \sim \beta_s$). On the other hand, when $\Lambda^{\pm}$ is small, the triple junction can strongly modify the motion of the grain boundaries and $\beta_d \neq \beta_s$ such that the absolute value of the rate of change of

grain area $\dot{A}_{tj}^{\pm}$ is slower than expected based on the common $\Lambda^{\pm}=\infty$ assumption. Combining the expressions for $\Lambda^{\pm}$, $\dot{A}_{tj}^{\pm}$, and $\dot{A}_b$ yields an expression for the normalized triple junction mobility $\Lambda_{\text{sim}}^{\pm}$, directly (and only) in terms of parameters directly obtainable from the simulations ($\dot{A}_{tj}^{+\,-}$, $\dot{A}_b$, $\beta_d^{\pm}$ and $\beta_s$)

$$\Lambda_{\text{sim}}^{\pm} = \frac{M_{tj}^{\pm} w}{M_b} = \left(\frac{\pi}{2}\right)\left(\frac{\dot{A}_{tj}^{\pm}}{\dot{A}_b}\right)\frac{1}{|\cos\beta_d^{\pm} - \cos\beta_s|} \tag{6}$$

The mobility ratio $\Lambda_{\text{an}}^{\pm}$ can also be calculated directly from the analytical result for the triple junction migration given the static and dynamic angles, $\beta_s$ and $\beta_d^{\pm}$:

$$\Lambda_{\text{an}}^{+} = \frac{M_{tj}^{+} w}{M_b} = \left|\frac{\beta_d^{+}}{\cos\beta_d^{+} - \cos\beta_s}\right| \tag{7a}$$

and

$$\Lambda_{\text{an}}^{-} = \frac{M_{tj}^{-} w}{M_b} = \left|\frac{\ln(\sin\beta_d^{-})}{\cos\beta_d^{-} - \cos\beta_s}\right| \tag{7b}$$

Equating the simulation and analytical expressions for the triple junction velocity gives the relationship between the rate of change of grain area and the triple junction angles:

$$\beta_d^{+} = \left(\frac{\pi}{2}\right)\frac{\dot{A}_{tj}^{+}}{\dot{A}_b} \tag{8a}$$

and

$$\beta_d^{-} = \sin^{-1}\left[\exp\left(\frac{\pi \dot{A}_{tj}^{-}}{2\dot{A}_b}\right)\right]. \tag{8b}$$

## 3. Simulation method

In this study, we perform molecular dynamics simulations to extract the triple junction mobility by measuring $\dot{A}_{tj}^{\pm}$ and the static and dynamic angles, $\beta_s$ and $\beta_d^{\pm}$. We measure these quantities as a function of the orientations of the bounding grains and temperature. The simulations were performed using the simple, well-characterized Lennard–Jones pair potential. This is a generic potential that allows easy assessment of a wide-range of materials by changing parameters in the results, rather than accurately describing any single material. Because the simulation geometries in Fig. 1 are inherently two dimensional, the simulations were performed in two dimensions (i.e. the XY plane). This was done for computational efficiency since a very large number of conditions had to be simulation (temperature, misorientation, geometries). For more details on the MD simulation technique employed, see Ref. 24. Energies are reported in units of the Lennard–Jones potential well depth $\epsilon$, distance in units of the equilibrium atom separation $r_0$, area in units of the perfect crystal area per atom $a_0$ and time in units of $\tau = (M_{at} r_0/\epsilon)^{1/2}$, where $M_{at}$ is the atomic mass. For example, in the case of A1, $\epsilon$=0.57 eV and $r_0$=2.86 Å. The potential was cut-off at $r_c$=2.1$r_0$, which is midway between the second and third nearest neighbors in the zero temperature equilibrium triangular lattice. A velocity-resealing thermostating algorithm was used to set the temperature [25]. Periodic boundary conditions were employed in the direction perpendicular to the straight boundaries in Fig. 1. In order to maintain the grain misorientations (especially at high temperature), the bottom three layers were frozen. Additionally, the X-coordinates of the atoms in the top three layers were fixed such that those atoms could move only in the Y-direction to accommodate the dilatational stresses generated due to the decrease in net boundary area during the simulation. Additional simulations were performed in the geometry of Figs. 1a and c with free surfaces on the top and sides to ensure that these boundary conditions did not significantly modify the results.

The initial atomic configurations were created by misorienting grains $b_1$ and $b_2$ with respect to grain $a$ by $\pm\theta$ and hence with respect to each other by $2\theta$, such that the grain boundary $b_1b_2$ is a symmetric boundary. This methodology enables the reduction of the description of the entire tri-crystallography in terms of a single misorientation variable, $\theta$. The simulation geometries were relaxed by performing molecular dynamics simulations at very low temperatures (0.010–0.025 $\epsilon/k_B$) prior to the grain boundary migration study to enable the atoms at the grain boundaries to equilibrate. The entire system is then heated slowly to the desired temperature in a step-wise fashion. The migration

rate $\dot{A}_{tj}^{\pm}$ is deduced from the slope of the area of the half-loop grain $\dot{A}_{tj}^{\pm}$ versus time $t$ plot. $\dot{A}_{tj}^{\pm}$ is simply the product of the number of atoms in the half-loop grain and the area per atom $a_0$. This requires the assignment of each atom in the simulation cell to one of the grains at each time, as described in detail in Ref. 24. The dynamic triple junction angle $\beta_d^{\pm}$ was extracted by measuring the angle subtended between the tangent of the *ab* grain boundary at the triple junction and the extension of the $b_1b_2$ boundary into grain $a$ (i.e., $\beta_{ab_1} + \beta_{ab_2} = 2\beta_d$, see Fig. 1a and Fig. 1b). $\dot{A}_{tj}^{\pm}$ and $\beta_{tj}^{\pm}$ measurements are only made during times for which the grain boundary(ies) enclosing the half-loop grain shrinks or grows in a steady-state, self-similar manner. The angles reported were averaged over several measurements during the course of each of 3 simulations performed for each set of conditions. The static equilibrium angles $\beta_s$ were determined by performing larger scale simulations at high temperatures until the boundaries have stopped migrating (see Ref. 26).

The dependence of triple junction mobility on grain boundary and triple junction crystallography is simulated in tri-crystals for a range of boundary misorientations. Special or singular boundaries (e.g. $\Sigma$=7, $\theta$=38.2° and $\Sigma$=13, $\theta$=32.21°, where $\Sigma$ is the inverse density of coincident sites), vicinal or near-singular boundaries (near $\Sigma$=7 and $\Sigma$=13), and general boundaries were all simulated. It should be noted that in the present 2-d triangular lattice simulations, where misorientations correspond to tilts about the ⟨111⟩ axis in the related fcc lattice, an $ab_1$ and $ab_2$ misorientation $\theta$ corresponding to $\Sigma_{ab}$, produces a $b_1b_2$ boundary corresponding to $\Sigma_{bb} = \Sigma_{ab}^2$. All misorientations $\theta$ were within the range $30° \leq \theta \leq 40°$, where the entire range of unique boundary misorientations lies between $30° \leq \theta \leq 60°$ which are symmetry-related to those with $30° > \theta > 0°$ in this lattice.

Triple junctions kinetics were also investigated as a function of grain size (half-loop width) and temperature. These simulations are performed for tri-crystallographies for which significant triple junction drag is observed. The simulations are performed for $19r_0 < w < 50r_0$ and $0.075\epsilon/k_B < T < 0.250\epsilon/k_B$. Activation energies for migration were extracted from the slope of the logarithm of the rate of change of half-loop area versus the inverse temperature. Three runs are performed for each simulation condition and the simulation parameters.

## 4. Results

Fig. 2 shows the atomic configurations corresponding to three different times ($t$=550$\tau$, 1245$\tau$ and 1750$\tau$), for a simulation performed for the + geometry at $T$=0.125$\epsilon/k_B$, a half-loop width of $w$=25$r_0$ and $\theta$=40°. Careful examination shows that the apart from small fluctuations, the curvatures of the constituent grain boundaries at the triple junctions remain constant, implying that the triple junc-

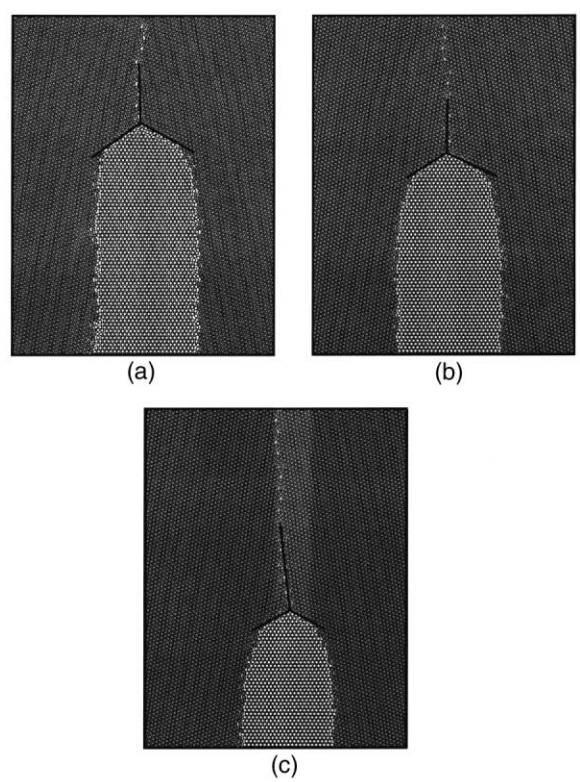


Fig. 2. The atomic configuration of a $\theta$=33° migrating triple junction ($T$=0.125$\epsilon/k_B$, $w$=25$r_0$) for the '+' simulation geometry at three instants of time: a) $t$=550$\tau$, b) $t$=1245$\tau$ and c) $t$=2550$\tau$. The bold lines indicate the tangents to the half-loop boundary at the triple junction. The dynamic triple junction angle was $\beta_{d^+}$=56° in a) $\beta_{d^+}$=58° in b) and $\beta_{d^+}$=58° in c).

tion migration is very nearly self-similar and, hence, steady-state, and that the triple junction angle is preserved throughout the simulation. Fig. 3 shows the atomic configurations for the simulation geometry in Fig. 1b ($t$=2000$\tau$ and $t$=14 000$\tau$) at the same temperature and half-loop width as in Fig. 2. Again, it is clear from the figure that the tri-crystal shape is self-similar during its migration.

The self-similarity of triple junction migration enables us to extract the triple junction migration rate in terms of the rate of change of the area of the half-loop grain, $\dot{A}_{tj}^{\pm}$. The temporal evolution of the grain areas for the structures in Fig. 1, are shown in Fig. 4 for the same conditions as in Figs. 2 and 3. It is important to note that for the '−' simulation geometry, the total calculated area corresponds to the sum of the areas of grains $b_1$ and $b_2$, which in turn is twice that of the half-loop area. The half-loop area decreases with time in a monotonic fashion, with some superimposed noise. At late times, the retracting half-loop is influenced by the frozen layer of atoms at the bottom of the simulation cell and, hence, no measurements were made there. Some of the fluctuations seen in Fig. 4 at intermediate time are associated with thermal transients in the shape of the half-loop and triple junction angle during half-loop retraction. More detailed discussion of the nature of the fluctuations/transients in the $\dot{A}_{tj}^{\pm}$ versus $t$ plots may be found elsewhere [24]. These transients are

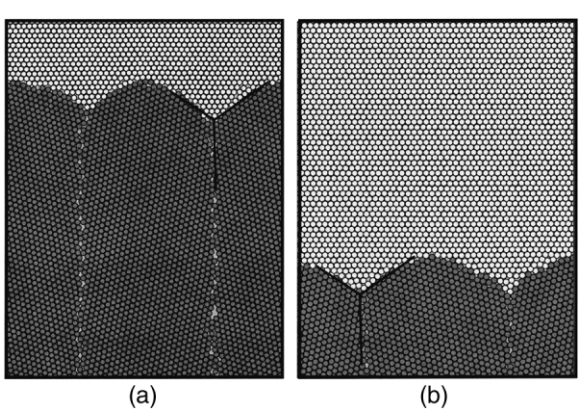


Fig. 3. Same as in Fig. 2, but for the '−' geometry. The atomic configurations correspond to instants of time: a) $t$=2000$\tau$ and b) $t$=14 000$\tau$. The dynamic triple junction angle was $\beta_{\bar{d}}$ =61° in a) and $\beta_{\bar{d}}$=62° in b).

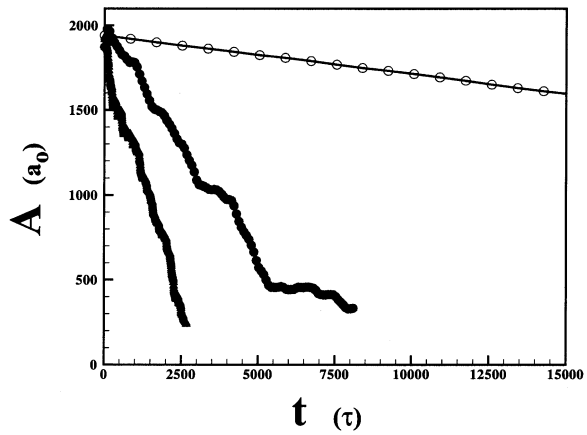


Fig. 4. The rate of change in the area of the half-loop grain (grain $a$ in Figs. 1a and c, and grain $b$ in Fig. 1b) with and without triple junctions for the same conditions as in Fig. 2. The filled and open circles indicate the '+' and '−' geometries, respectively, and the shaded triangles indicate the results of the bi-crystal simulation.

excluded from the determination of the steady-state slope $\dot{A}_{tj}^{\pm}$. The regions of steady-state migration are characterized by constant $\beta_d^{\pm}$ as well as a linear $\dot{A}_{tj}^{\pm}$ versus $t$ plot. For the simulation conditions corresponding to Figs. 2 and 3, the extracted rates of change of the half-loop grain area are $\dot{A}_{tj}^{+} = 0.33 \pm 0.06 a_0/\tau$ and $\dot{A}_{tj}^{-} = 0.024 \pm 0.009 a_0/\tau$. The difference between the two values of $\dot{A}_{tj}^{\pm}$ is expected based upon the differences in geometry, as represented by the differences between Eqs. (5a) and (5b).

Fig. 4 also shows simulation data obtained from the bi-crystal half-loop (i.e., without a triple junction) simulations (see Fig. 1c), $A_b$ vs. $t$, for the same ($ab$) misorientation, temperature and half-loop width as for the triple junction migration simulations. The slope of this curve is $\dot{A}_b = 0.54 \pm 0.03 a_0/\tau$ [24,26]. Comparing $\dot{A}_{tj}^{\pm}$ and $\dot{A}_b$, we find that $\dot{A}_{ij}^{-} < \dot{A}_{ij}^{+} < \dot{A}_b$. For the simulations shown in Figs. 2 and 3, the average dynamic triple junction angles are $\beta_d^{+} = 59° \pm 1°$ and $\beta_d^{-} = 62° \pm 1°$. The static triple junction angle for this tri-crystallography has been previously determined to be $\beta_s = 61° \pm 1°$. Hence, for this tri-crystal, the dynamic triple junction angle $\beta_d^{\pm}$ is approximately same as $\beta_s$.

Figs. 5 and 6 show the atomic configurations during triple junction migration in both the '+' ($t$=450$\tau$ and 2550$\tau$) and '−' ($t$=3000$\tau$ and 25 000$\tau$) directions respectively, under the same conditions as Fig. 2 and Fig. 3, but for $\theta$=38.2°. This angle corresponds to a high symmetry, low $\Sigma$ (i.e., $\Sigma$7) misorientation. Once again, it is clear that the triple junction migration takes place in a nearly self-similar fashion, with constant $\beta_{tj}^{\pm}$. The temporal evolution of the areas of the half-loop grains for the tri-crystal simulations shown in Figs. 5 and 6 as well as the corresponding bi-crystal simulations is shown in Fig. 7. Averaged over three different simulation runs, the steady-state slopes of the $\dot{A}_{tj}^{\pm}$ versus $t$ plots for the '+' and '−' geometries are $\dot{A}_{tj}^{+} = 0.64 \pm 0.05 a_0/\tau$ and $\dot{A}_{tj}^{-} = 0.039 \pm 0.006 a_0/\tau$. The rate of change of area for the bicrystal half-loops at $\theta$=38.2° is $\dot{A}_b = 1.32 \pm 0.08 a_0/\tau$ [24,26]. The dynamic triple junction angles for the '+' and '−' geometry are measured to be $\beta_d^{+} = 47° \pm 1°$ and $\beta_d^{-} = 72° \pm 1°$ respectively. For this tri-crystallography, the static triple junction angle is $\beta_s = 60 \pm 2°$. Unlike for the low symmetry $\theta$=40° case, where the triple junction angles were nearly the same in the '+' and '−' geometries, in the $\theta$=38.2° case the triple junction angles are much different ($\Delta\theta$=25°±2°), implying that in the $\theta$=38.2° case, triple junction drag may be substantial.

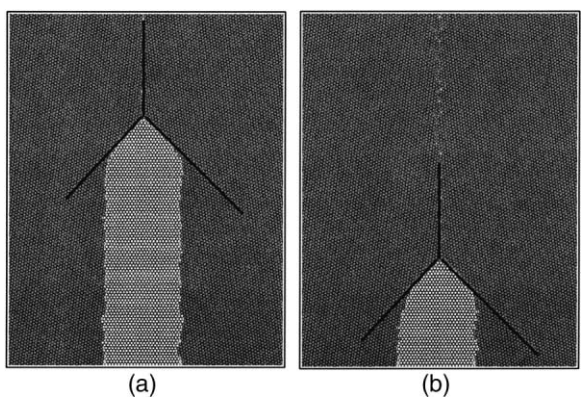


Fig. 5. Atomic configurations during the migration of a $\theta$=38.2° ($\Sigma$=7) '+' geometry triple junction ($T$=0.125$\epsilon/k_B$, $w$=25$r_0$) at two instants of time: a) $t$=450$\tau$ and b) $t$=2150$\tau$. The dynamic triple junction angles were measured to be $\beta_d^{+}$=47° in a) and $\beta_d^{+}$=48° in b).

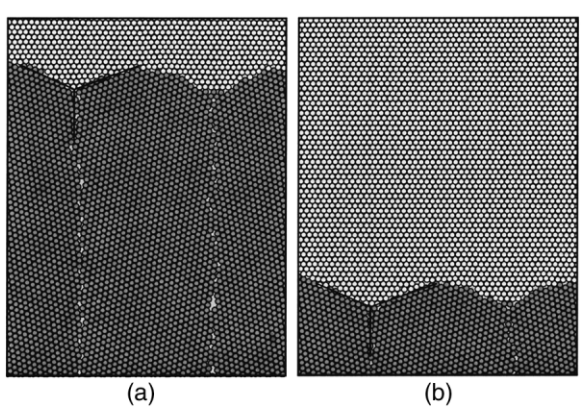


Fig. 6. Same as in Fig. 5, but for the '−' geometry. The dynamic triple junction angles were measured to be $\beta_d^{-}$=72° in a) and $\beta_d^{-}$=71° in b).

Triple junction migration simulations were performed for a total of 13 different grain boundary misorientations $\theta$ at fixed width ($w$=25$r_0$) and temperature ($T$=0.125$\epsilon/k_B$). The extracted simulation parameters ($\dot{A}_{tj}^{\pm}$, $\dot{A}_b$, $\beta_d^{\pm}$ and $\beta_s$), averaged over three independent simulation runs, are tabulated in Table 1 as a function of $\theta$. Depending on the misorientation, $\dot{A}_{tj}^{\pm}$ and $\dot{A}_b$ can be very similar or very different (by as much as a factor of two). This difference is largest for low $\Sigma$ (singular) boundaries. On the other hand, $\dot{A}_{tj}^{-}$ is always approximately an

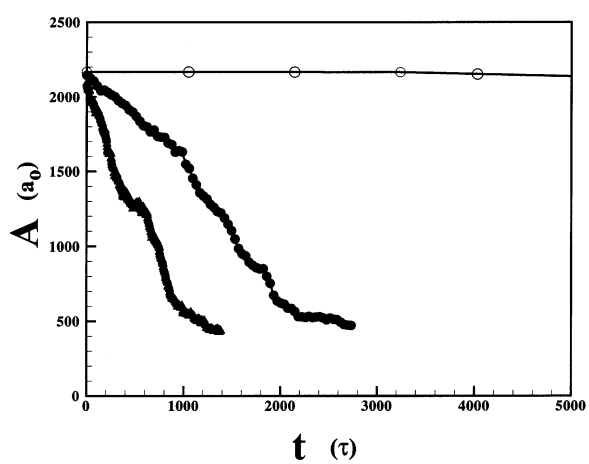


Fig. 7. The rate of change in the area of the half-loop grai with and without triple junctions for the same conditions as in Fig. 5. The filled and open circles indicate the '+' and '−' geometries, respectively, and the shaded triangles indicate the results of the bi-crystal simulation.

Table 1
The tabulated values of the extracted rate of change of area of the half-loop grain during the triple junction migration for '+' and '−' geometry, $\dot{A}_{tj}^{+}$ and $\dot{A}_{tj}^{-}$, rate of change of area of the half-loop grain extracted from bi-crystal simulations [26]), $\dot{A}_b$, the dynamic and static triple junction angles $\beta_d^{\pm}$ and $\beta_s$ as a function of the grain boundary *ab* misorientation $\theta$

| $\theta$ (°) | $\dot{A}_{tj}^{+}(a_0/\tau)$ | $\dot{A}_{tj}^{-}(a_0/\tau)$ | $\dot{A}_b(a_0/\tau)$ | $\beta_d^{+}$ (°) | $\beta_d^{-}$(°) | $\beta_s$(°) |
|---|---|---|---|---|---|---|
| 31.50 | 0.31±0.009 | 0.039±0.009 | 0.48±0.01 | 59±1 | 61±1 | 60±1 |
| 32.00 | 0.27±0.009 | 0.035±0.007 | 0.45±0.04 | 57±1 | 65±1 | 60±1 |
| 32.21 | 0.16±0.012 | 0.005±0.001 | 0.32±0.04 | 44±1 | 74±1 | 60±1 |
| 33.00 | 0.29±0.021 | 0.036±0.013 | 0.46±0.03 | 53±1 | 68±1 | 60±2 |
| 33.57 | 0.28±0.020 | 0.043±0.012 | 0.45±0.04 | 56±1 | 64±1 | 60±1 |
| 34.00 | 0.33±0.009 | 0.042±0.008 | 0.50±0.04 | 59±1 | 62±1 | 61±1 |
| 35.57 | 0.39±0.021 | 0.070±0.011 | 0.59±0.04 | 58±1 | 62±1 | 60±1 |
| 37.00 | 0.47±0.033 | 0.088±0.021 | 0.75±0.03 | 59±1 | 62±1 | 60±1 |
| 37.52 | 0.45±0.031 | 0.043±0.009 | 0.78±0.02 | 54±1 | 67±1 | 60±1 |
| 38.22 | 0.64±0.051 | 0.039±0.006 | 1.32±0.03 | 47±1 | 72±1 | 60±1 |
| 38.98 | 0.52±0.038 | 0.041±0.007 | 0.89±0.02 | 50±1 | 67±1 | 61±1 |
| 39.50 | 0.45±0.024 | 0.043±0.008 | 0.68±0.01 | 59±1 | 63±1 | 62±1 |
| 40.00 | 0.33±0.019 | 0.046±0.009 | 0.54±0.03 | 58±1 | 62±1 | 61±1 |

order of magnitude lower than $\dot{A}_b$ for all misorientations. The static triple junction angles are nearly independent of misorientation in this two-dimensional, Lennard–Jones system and are very close to the isotropic limit of $\beta_s$=60°. The dynamic triple junction $\beta_d^+$ varies from a low of 44°±1° to a high of 59°±1°, and from a low of 60°±1° to a high of 74°±1° for the '−' geometry. Of more importance than the absolute value of the dynamic triple junction angle is the deviation of this angle from its equilibrium value, $|\beta_d^{\pm} - \beta_s|$. While little or no deviations (within the error bars) of the dynamic triple junction angles from the static value of 60° are common in the simulation performed, significant deviations do occur at or very near low $\Sigma$ misorientations: $|\beta_d^+ - \beta_s| = 16°$ and $|\beta_d^- - \beta_s| = 14°$ for $\Sigma$13($\theta$=32.2°) and $|\beta_d^+ - \beta_s| = 13°$ and $|\beta_d^- - \beta_s| = 1°$ for $\Sigma$7 ($\theta$=38.2°). The observation of large deviations of the dynamic angle from their equilibrium values appears strongly correlated with large deviations of $\dot{A}_{tj}^{\pm}$ from $\dot{A}_b$ . We return to this point below.

We now investigate the dependence of the deviation of the dynamic triple junction angles from their equilibrium values $|\beta_d^{\pm} - \beta_s|$ on the half-loop width $w$. We performed simulations for the tri-crystal geometries of Figs. 1a and b corresponding to the low $\Sigma$ orientation $\theta$=38.2° ($\Sigma$7) at $T$=0.125$\epsilon/k_B$, for half-loop widths in the range $20r_0 \leq w \leq 50r_0$. $\dot{A}_{tj}^{\pm}$ and $\beta_d^{\pm}$ are tabulated in Table 2 for each width and the two geometries. The rate of shrinkage of the half-loop in the bicrystal simulations (Fig. 1c) is independent of half-loop width, $\dot{A}_b$, for all half-loop widths considered here [26]. The variation of the dynamic angle $\beta_d^{\pm}$ (as measured from figures such as Fig. 2 and Fig. 3) with half-loop width is shown in Fig. 8. As the half-loop width increases, the deviation $|\beta_d^{\pm} - \beta_s|$ decreases for both the '+' and '−' geometries. For widths above approximately $40r_0$, the dynamic angle $\beta_d^{\pm}$ is nearly indistinguishable from the static equilibrium value, $\beta_s = 60° \pm 1°$. $\beta_d^{\pm}$ can also be calculated directly from the rate of change of the half-loop area using Eqs. (8a) and (8b) and the reduced mobility of the half loop. Eqs. (8a) and (8b) also show $\beta_d^{\pm}$ determined in this manner, as a function of half-loop width. Clearly the two methods for determining $\beta_d^{\pm}$ are in agreement, indicating the validity of the theoretical treatment and confirming that for $w \geq 40r_0$, both $\beta_d^{\pm}$ and $\dot{A}_{tj}^{\pm}$ approach their expected equilibrium values. This data suggests that at small $w$ triple junction drag is significant.

The effect of temperature on triple junction migration is investigated by performing simulations on low $\Sigma$ (i.e., $\Sigma$7, $\theta$=38.2°) tri-crystals with a half-loop width of $w$=25$r_0$ at different temperatures. The half-loop retraction rates $\dot{A}_{tj}^{\pm}$ and $\dot{A}_b$ and triple junction angles $\beta_d^+$ for $0.075\epsilon/k_B \leq T \leq 0.250\epsilon/k_B$ are tabulated in Table 3. Fig. 9 shows the variation of $\beta_d^+$ with the temperature $T$, where $\beta_d^+$ has been directly measured from images of the migrating triple junction and deduced from Eqs. (8a) and (8b). Within the error bars of the determination of $\beta_d^+$ , both methods yield the same values. As the temperature increases, the deviation of the dynamic angle from the static angle $|\beta_d^+ - \beta_s|$ decreases. Similar trends are also observed for the '−' geometry of Fig. 1b. Thus increasing the temperature has the same effect as increasing the width of the half-loop. In short, substantial deviations of $\beta_d^{\pm}$ from its equilibrium value $\beta_s$ only occur for special misorientations, small grain size and relatively low temperature.

## 5. Discussion

Our results show that for low $\Sigma$ misorientations and misorientations near these, the dynamic triple junction angles deviate significantly from their equilibrium values. This results in significantly slower boundary migration in the tri-crystal geometries, as indicated by the extracted values of the rates of change of areas of the half-loop grain, $\dot{A}_{tj}^{\pm}$ . Instead of focusing on the triple junction mobility itself, it is more interesting to examine the triple junction mobility relative to the mobility of the grain boundaries it bounds. The appropriate dimensionless ratio $\Lambda^{\pm}$ can be derived from the simulations using two distinct approaches: by directly measuring $\dot{A}_{tj}^{\pm}$, $\dot{A}_b$, $\beta_d^{\pm}$ and $\beta_s$ from simulations $\Lambda_{\mathrm{sim}}^{\pm}$ (see Eq. (6)) and by a combination of the analytical results of Galina et al. [20] and simulation results $\Lambda_{\mathrm{an}}^{\pm}$ (see Eqs. (7a) and (7b)). As

Table 2
The values of the rate of change of area of the half-loop grain $\dot{A}_{tj}^{\pm}$ and the dynamic triple junction angle $\beta_d^{\pm}$ as a function of the half-loop width $w$ for both the triple junction geometries shown in Figs. 1a and b, with grain boundary $ab$ misorientation $\theta$=38.2° ($\Sigma$=7) and at temperature $T=0.15\epsilon/k_B$

| $w$ ($r_0$) | $\dot{A}_{tj}^{+}$ ($a_0/\tau$) | $\beta_d^{+}$ (°) | $\dot{A}_{tj}^{+}$ ($a_0/\tau$) | $\beta_d^{-}$ (°) |
|---|---|---|---|---|
| 19 | 0.63±0.08 | 46±1 | 0.029±0.006 | 73±1 |
| 21 | 0.65±0.03 | 46±1 | 0.031±0.008 | 73±1 |
| 23 | 0.67±0.05 | 47±1 | 0.029±0.007 | 72±1 |
| 25 | 0.64±0.08 | 47±1 | 0.039±0.009 | 72±1 |
| 29 | 0.70±0.06 | 47±1 | 0.045±0.008 | 69±1 |
| 31 | 0.72±0.07 | 50±1 | 0.058±0.009 | 67±1 |
| 33 | 0.78±0.04 | 53±1 | 0.072±0.009 | 66±1 |
| 35 | 0.83±0.07 | 56±1 | 0.082±0.009 | 63±1 |
| 37 | 0.86±0.03 | 58±1 | 0.095±0.009 | 61±1 |
| 40 | 0.86±0.05 | 59±1 | 0.097±0.008 | 61±1 |
| 45 | 0.92±0.07 | 59±1 | 0.110±0.018 | 61±1 |
| 50 | 0.91±0.07 | 59±1 | 0.100±0.020 | 61±1 |

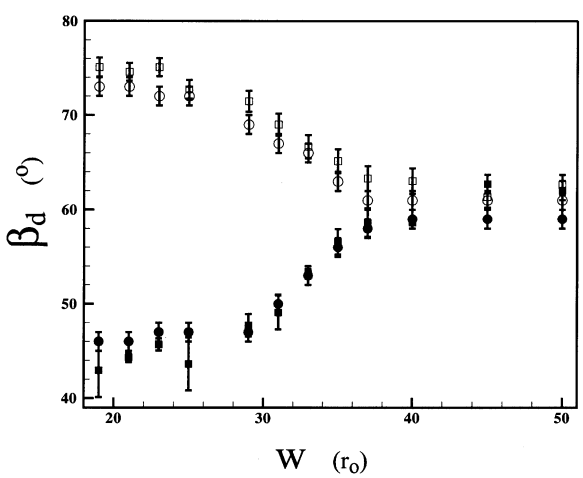


Fig. 8. The dynamic triple junction angle $\beta_d^{\pm}$ plotted as a function of the half-loop grain width $w$, for both the '+' (filled symbols) and '−' (open symbols) geometries and for simulation conditions $\theta$=38.2° and $T=0.125\epsilon/k_B$. The circles indicate the directly measured dynamic angles while the squares correspond to $\beta_d^{-}$ from Eqs. (8a) and (8b).

discussed above, when $\Lambda^{\pm}$ is small, the low relative intrinsic triple junction mobility can yield substantial drag and slow the rate of migration in systems with triple junctions.

Using the $\dot{A}_{tj}^{\pm}$, $\dot{A}_b$, $\beta_d^{\pm}$ and $\beta_s$ data contained in Table 1, we determine $\Lambda_{sim}^{\pm}$ and $\Lambda_{an}^{\pm}$ as a function of grain boundary misorientation. The variation of these two parameters with the $ab$ grain boundary misorientation angle $\theta$ for the '+' and '−' geometries are shown in Fig. [10]. As expected, the two methods used to extract $\Lambda^{\pm}$ yield nearly indistinguishable results. The variation of $\Lambda^{\pm}$ with misorientation shown in Fig. 10 is not monotonic, but rather exhibits distinct minima for low $\Sigma$ misorientations. For the $\Sigma$7 misorientation, $\Lambda_{sim}^{+} = 4.181$ and $\Lambda_{sim}^{-} = 0.24$, while for the low $\Sigma$=13 misorientation $\Lambda_{sim}^{+} = 3.58$ and $\Lambda_{sim}^{-} = 0.11$. Similar values were obtained for $\Lambda_{an}^{+}$ and $\Lambda_{an}^{-}$. While the data presented in Fig. 10 suggest that these minima are rounded rather than true cusps (this is perhaps due to small model size), it is not possible to make an unambiguous determination on the basis of the limited number of data points in Fig. 10 (we do note, however, that the boundary energy versus misorientation does appear to show real cusps [27]). Nonetheless, it is clear that the low $\Sigma$ misorientations are indeed special. Since the values of $\Lambda^{\pm}$ at these minima are of order unity, the intrinsic triple junction mobility ($M_{tj}^{\pm} w$) is comparable to the intrinsic mobilities of the grain boundaries that bound it. This observation, coupled with Eq. (4) implies that for tri-crystallographies corresponding to low $\Sigma$ misorientations, triple junctions can exert significant drag on the motion of grain boundaries.

Data presented above (Fig. 8) demonstrated that the dynamic triple junction angle for the low $\Sigma$7 misorientation deviates substantially from its equi-

Table 3
The values of the rate of change of area of the half-loop grain during the triple junction (+ geometry) and bi-crystal simulations, and the dynamic triple junction angle $\beta_d^+$ as a function of simulation temperature $T$ for the grain boundary $ab$ misorientation $\theta$=38.2° ($\Sigma$=7) and half-loop width $w=25r_0$

| $T$ ($\epsilon/k_B$) | $\dot{A}_{tj}^+$ ($a_0/\tau$) | $\dot{A}_b(a_0/\tau)$ | $B_d^+$ |
|---|---|---|---|
| 0.75 | 0.16±0.082 | 0.33±0.083 | 45±2 |
| 0.100 | 0.29±0.095 | 0.58±0.091 | 45±2 |
| 0.125 | 0.64±0.121 | 1.32±0.110 | 46±2 |
| 0.150 | 0.91±0.132 | 1.81±0.111 | 47±3 |
| 0.200 | 1.69±0.122 | 3.03±0.098 | 51±2 |
| 0.225 | 2.66±0.192 | 4.36±0.142 | 55±2 |
| 0.250 | 3.59±0.310 | 5.80±0.160 | 56±2 |

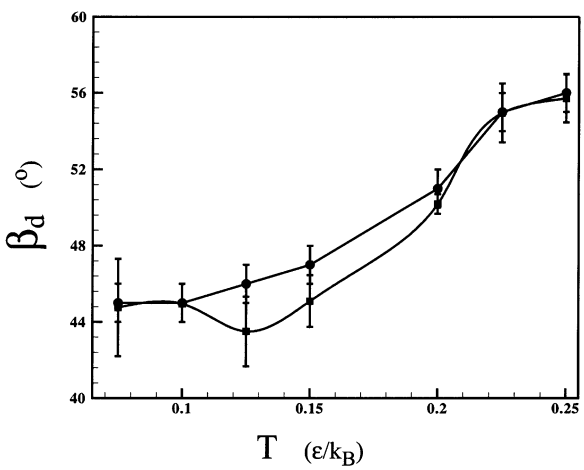


Fig. 9. The dynamic triple junction angle $\beta_d^+$ versus temperature $T$, for the '+' geometry and for simulation conditions $\theta$=38.2° and $T$=0.125$\epsilon/k_B$. The circles indicate the directly measured dynamic angles while the squares correspond to $\beta_d^+$ from Eqs. (8a) and (8b).

librium value at small grain size (half-loop width) but not at large grain size. This suggests that triple junction drag is significant at small half-loop width. We examine this suggestion by considering the variation of $\Lambda_{sim}^+$ with half-loop grain width in Fig. 11. For $w<30r_0$ at this temperature, the normalized triple junction mobility is $\Lambda_{sim}^+\cong 4$. However, $\Lambda_{sim}^+$ increases rapidly in the range $30r_0<w\leq 40r_0$ and then saturates at a large value $\Lambda_{sim}^+\approx 70$. Similar trends were also observed for $\Lambda_{an}^+$. This increase in $\Lambda_{sim}^+$ cannot be attributed solely to the linear term in $w$ in the definition of $\Lambda_{sim}^+ = M_{tj}w/M_b$. Since $M_b$ is independent of half-loop width (at these widths) [24,26], this strong variation must be a result of the variation in the intrinsic triple junction mobility $M_{tj}$. This implies that for small grain sizes, the triple junction can create significant drag on boundary migration. However, as the width is increased above a critical value, triple junction drag rapidly diminishes.

Fig. 10 showed that the dynamic triple junction angles exhibit large deviations from its equilibrium value at low temperature. The magnitude of this deviation decreased with increasing temperature. A reflection of this effect in the normalized triple junction mobility with temperature is shown in Fig. 12a, where we plot $\ln(\Lambda_{sim}^+)$ versus $1/T$. For low temperatures ($T<0.075\epsilon/k_B$), $\Lambda_{sim}^+\cong 4$ and $\Lambda_{sim}^+\cong 16$ increases to as the temperature is raised to $T$=0.250$\epsilon/k_B$ ($\cong 0.67T_m$). The data in Fig. 12a shows two distinct slopes indicating two distinct regimes of behavior. At low temperature, $\Lambda_{sim}^+$ is small, indicating that the motion of the half-loop with the triple junction is controlled by the triple junction. At high temperature, $\Lambda_{sim}^+$ is substantially larger and the motion is controlled by the mobility of the grain boundaries. The difference in slope between these two regimes is substantial; the high temperature slope is approximately seven times larger than at low temperature. The simulation data presented in Fig. 12a are consistent with recent experimental measurements of triple junction drag in high purity $<10\bar{1}0>$-oriented Zn in a geometry equivalent to that of Fig. 1a, with 60° misoriented $ab$ tilt-boundaries, by Czubayko et al. [18]. The triple junction angle $\beta_d^+$ in these experiments was observed to increase with increasing

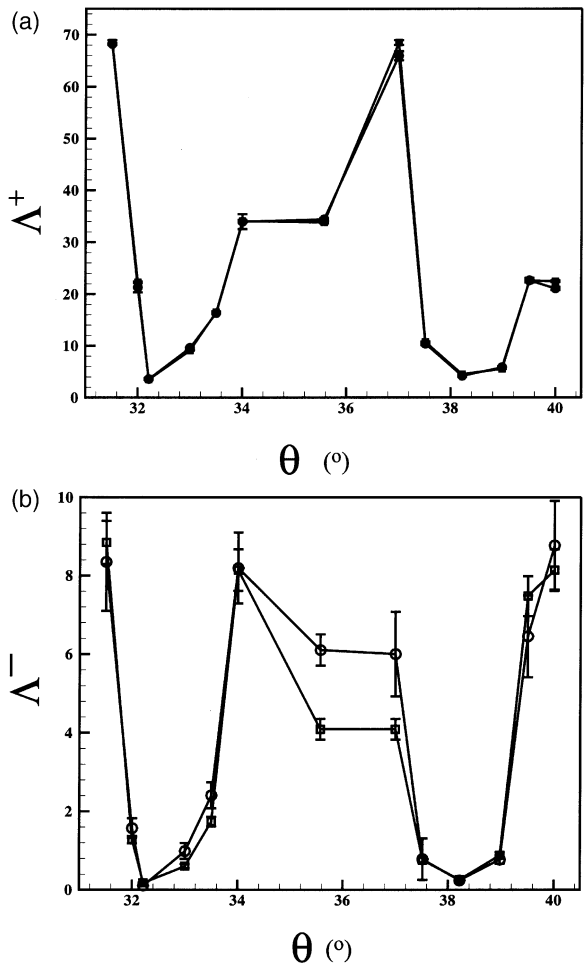


Fig. 10. a) The dimensionless triple junction mobility parameter, $\Lambda^+$ as a function of the *ab* grain boundary misorientation $\theta$ for the '+' geometry, $w=25r_0$ and $T=0.125\ \epsilon/k_B$. The circles and squares indicate $\Lambda^+_{sim}$ and $\Lambda^+_{in}$, respectively. b) Same as a), but for the '−' geometry, where the circles indicate $\Lambda^-_{sim}$ while the squares indicate $\Lambda^-_{in}$.

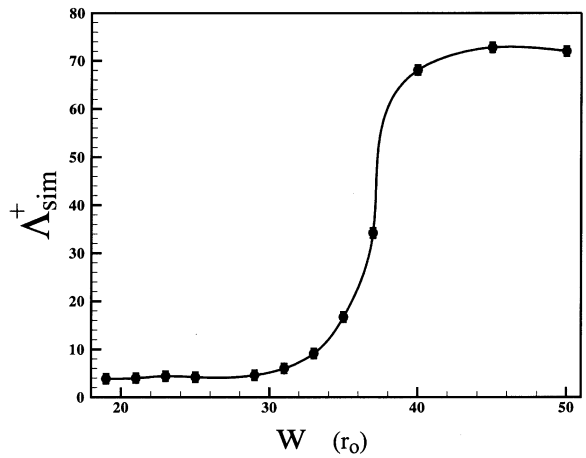


Fig. 11. The dimensionless triple junction mobility parameter, $\Lambda^+_{sim}$, versus the half-loop width $w$ for the '+' geometry, $\theta=38.2°$ and $T=0.125\epsilon/k_B$.

temperature and a plot of $\ln(\Lambda^+_{exp})$ versus $1/T$ also shows two distinct slopes, with that at low temperature nearly ten times smaller than that at high temperature (see Fig. 12b).

The simulation and experimental results are both consistent and somewhat surprising. In the low temperature regime, where motion is controlled by the triple junctions, we expect the slopes to be large (the activation energy for triple junction migration is greater than that for grain boundary migration) but it is found to be small. Similarly, in the high temperature regime, where migration is controlled by the grain boundary mobility, the slope is large instead of, as we expect, small. These results can be rationalized by consideration of Eqs. (7a) and (7b), which shows that $\Lambda$ can be described completely in terms of the dynamic triple junction angle. Consider the limiting case where the triple junction mobility tends to zero. Clearly the triple junction angle is not the equilibrium value (which requires high mobility) and is determined by the motion of the grain boundary. In this limit, the dynamic angle is determined by the boundary mobility even though the overall half-loop migration rate is limited by the triple junction mobility. Therefore, in the low temperature limit, the temperature dependence of $\Lambda$ is set by the activation energy for boundary mobility. Similarly, at high temperature where the rate of half-loop shrinkage is determined by the boundary mobility ($\Lambda>1$), the temperature dependence of the triple junction angle is determined by the activation energy for triple junction mobility.

The data presented above indicate that the triple junction mobilities and dynamic wetting angles depend on the direction of triple junction migration. We quantify this effect by plotting the ratio of these mobilities for motion in opposite directions ($M^-_{tj}/M^+_{tj}$) versus the *ab* grain boundary misorientation $\theta$ in Fig. 13. The plot shows that

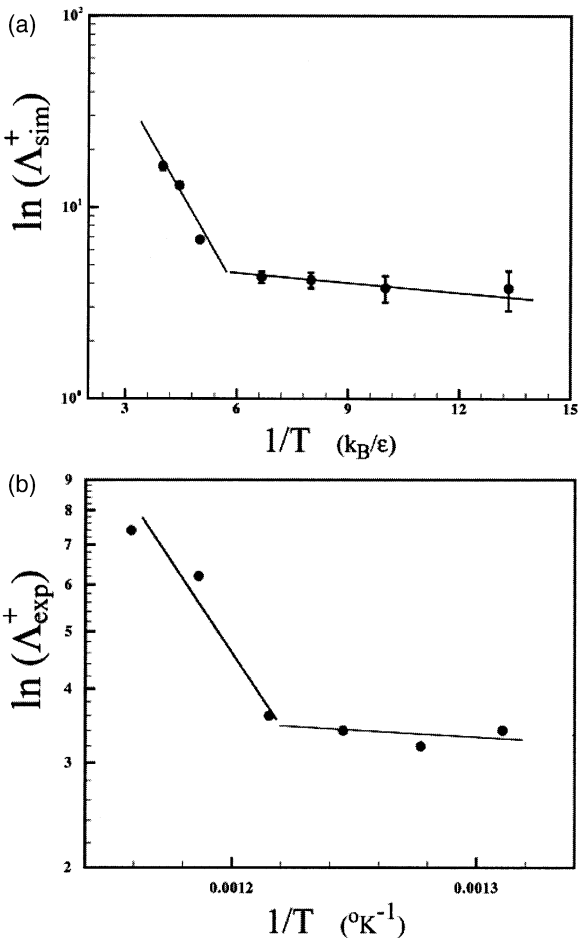


Fig. 12. a) The logarithm of the dimensionless triple junction mobility parameter, $\Lambda^+_{sim}$, versus the inverse temperature for the '+' geometry, $\theta$=38.2° and $w$=25$r_0$. b) Same as in a) for the experimental data $\Lambda^+_{exp}$ on high purity $< 1010 >$ -oriented Zn with 60° misoriented *ab* tilt-boundaries, by Shvindlerman et al. [20]. In both cases, the lines are guides for the eye.

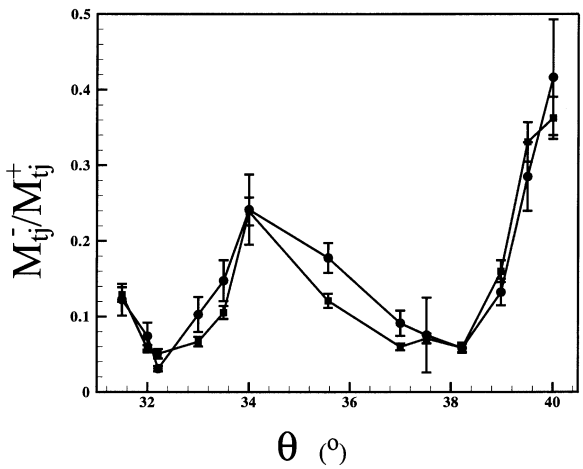


Fig. 13. The ratio of the triple junction mobilities extracted for the '+' and '−' geometries plotted as a function of *ab* grain boundary misorientation $\theta$ for $w$=25$r_0$ and $T$=0.125$\epsilon/k_B$. The circles indicate $\Lambda^-_{sim}/\Lambda^+_{sim} = (M^-_{ij}/M^+_{ij})_{\rm sim}$ while the squares indicate $\Lambda^-_{an}/\Lambda^+_{an} = (M^-_{ij}/M^+_{ij})_{\rm an}$.

the intrinsic mobility of the triple junction in the direction that destroys the $b_1b_2$ boundary (i.e., the '−' geometry) is consistently smaller than the intrinsic mobility for triple junction migration in the direction that increases the length of the $b_1b_2$ boundary (i.e., the '+' geometry) for all the tricrystallographies simulated. This difference is largest under conditions where triple junction drag is most severe (i.e., in the vicinity of low $\Sigma$ boundaries). This ratio can be as large as 0.5 for cases where the triple junction has no effect on boundary migration, to as low as 0.05 for cases where significant triple junction drag is observed. This asymmetry in triple junction mobility is consistent with recent experimental observations of triple junction migration in high purity A1 by Molodov [28]. In these experiments, triple junction migration in the '+' geometry was easily measured, while in the '−' geometry under the same conditions quantitative measurements were difficult because the triple junction migrated at extremely low rate.

The triple junction migration in the '+' geometry involves the creation of a $b_1b_2$ boundary at the triple junction, while in the geometry represented by Fig. 1b, the triple junction motion destroys the $b_1/b_2$ boundary. The data presented above suggests that it is easier to create an $a_1/a_2$ boundary at the triple junction than destroy it. Clearly, destroying the $b_1/b_2$ boundary as the triple junction moves requires the transition of the material initially in the boundary from a relatively low symmetry arrangement into a highly ordered, crystalline one. Intuitively, this should be more difficult than the converse.

In centro-symmetric materials, simply changing the sign of the direction of motion should leave the triple junction mobility unaffected. While the crystal structure employed in these simulations is

indeed centro-symmetric, the tri-crystal structure is not. Nonetheless, detailed balance and classical rate theory considerations suggest that the forward and backward mobilities should be identical. These analyses are all based on the assumption that each of the intermediate states associated with the triple junction migration are in equilibrium with one another. This assumption can easily breakdown when the driving forces are large and/or the energy landscape is complex. As shown above, triple junction mobility is only important for boundary migration for small values of $\Lambda$. Such small values are only observed when the driving forces are large (small $w$) and the temperature is low. While it is not possible to accurately measure the triple junction mobility when the driving forces are small in the present simulations, we do find that the magnitude of the discrepancy between the forward and backward triple junction mobilities decreases as the driving force decreases. These observations suggest that while steady-state triple junction migration is possible under high driving forces, local equilibrium at the triple junctions is not maintained.

## 6. Conclusions

The main conclusion of the present study is that triple junction mobility is finite and can be sufficiently small to limit the rate of grain boundary migration. The drag on grain boundaries due to limited triple junction mobility is especially important at small grain sizes, low temperature and near high symmetry misorientations. Under these conditions, the triple junction angle $\beta_d$ also shows substantial deviations from its equilibrium, static value, $\beta_s$. $\beta_d$ can be either larger or smaller than $\beta_s$, depending on the tri-crystal geometry. Triple junction drag induces a dynamic force on the migrating triple junction that modifies the equilibrium Young–Duprè relation and thereby changes the triple junction angle. The effect of grain size on determining the importance of triple junction drag can be understood by recalling that larger grain sizes imply lower grain boundary velocities in curvature driven boundary migration. It easier for the low mobility triple junction to keep up with the moving boundaries when those boundaries are migrating slowly. Similarly, triple junction drag is of less importance at high temperature than at low temperature because triple junction mobility increases with increasing temperature. One interesting feature of the present results is that the triple junction mobility depends upon the direction that the triple junction migrates. This is not simply related to the possibility that the Onsager coefficient tensor may have off-diagonal components since the mobility depends on the sign of the triple junction motion. Rather it is more likely attributable to the non-equilibrium nature of triple junction migration under conditions where the drag is large.

The present simulations confirm the experimental observations of non-equilibrium triple junction angles and substantial triple junction drag seen in recent experiments [18]. One discrepancy between the experiments and simulations is the conditions under which triple junction drag is significant. In the present simulations, triple junction drag was never found to substantially retard boundary migration at grain sizes above approximately fifty inter-atomic spacings. On the other hand, the experiments have demonstrated triple junction drag for grain sizes in excess of 10 μm. This difference is likely attributable to the presence of impurities on the grain boundaries in the experiments, while the simulations model (intrinsic) migration in an ideally pure material. This suggests that impurity effects, even in extremely high purity materials, may substantially effect grain boundary and triple junction migration, because of segregation effects. Nonetheless, triple junction drag must always be considered when dealing with the very small grain sizes common to modern nano-structured materials and thin films.

## Acknowledgements

M.U. and D.J.S. gratefully acknowledge the financial support of the Division of Materials Science of the Office of Basic Energy Sciences of the United States Department of Energy (Grant DE-FG02-99ER45797), under whose auspices this research was performed. L.S.S. and G.G. express

their gratitude to the Deutsche Forschungsgemeeinschaft (DFG Grant 438 113/130/0) and to the Russian Foundation for Fundamental Research under contract N 96-02-17483 for financial support of their collaboration.

## References

[1] Ho E, Weatherly GC. Acta Metall. 1975;23:1451.
[2] Palumbo G, Doyle DM, Sherik AME, Erb U, Aust KT. Scripta Metall. Mater. 1991;25:679.
[3] Yoo MH, Trinkaus H. Mett. Trans. 1983;A14:547.
[4] Palumbo G, Aust KT. Mater. Sci. Eng. 1989;A113:139.
[5] Hashimoto S, Fujii TK, Miura S. Scripta Metall. 1987;21:169.
[6] King AH. Interface Sci. 1999;7:251.
[7] Frank FC. Acta Crystall. 1951;4:497.
[8] Srolovitz DJ, Sridhar N, Hirth JP, Cahn JW. Scripta Mater. 1998;39:379.
[9] Singh V, King AH. Scripta Mater. 1996;34:1723.
[10] Perevezentsev VN, Shcherban MY. Sov. Sol. Phys. 1998;5:36.
[11] Kopetskii CV, Fionova LK. Sov. Sol. Phys. 1982;12:111.
[12] Srinivasan SG, Cahn JW, Jonsson H, Kalonji G. Acta Metall. 1999;47:2821.
[13] Caro A, Van Swygenhoven H. Phys. Rev. 2001;B63:4101.
[14] Herring C. In: Kingston WE, editor. The physics of powder metallurgy. New York: McGraw-Hill; 1951. p. 14-3.
[15] Mullins WW. J. Appl. Phys. 1956;27:900.
[16] Dussan EB. Ann. Rev. Fluid Mech. 1979;11:371.
[17] Anderson DM, Worster MG, Davis SH. J. Cryst. Growth 1996;163:329.
[18] Czubayko U, Sursaeva VG, Gottstein G, Shvindlerman LS. Acta Mater. 1998;46:5863.
[19] Turnbull D. Trans. AIME 1951;191:661.
[20] Galina AV, Fradkov VY, Shvindlerman LS. Phys. Met. Metall. 1987;63:1220.
[21] Gottstein G, Shvinderman LS. Grain boundary migration in metals: thermodynamics, kinetics and applications. Boca Raton (FL): CRC Press, 1999.
[22] Gottstein G, Sursaeva V, Shvindlerman LS. Interface Sci. 1999;7:273.
[23] Aristov VY, Fradkov VE, Shvindlerman LS. Sov. Sol. Phys. 1980;22:1055.
[24] Upmanyu M, Smith RW, Srolovitz DJ. Interface Sci. 1998;6:41.
[25] Allen MP, Tildesley DJ. Computer simulation of liquids. Oxford: Clarendon, 1987.
[26] Upmanyu M, Srolovitz DJ, Shvindlerman LS, Gottstein G. Interface Sci. 1999;7:307.
[27] Srolovitz DJ, Upmanyu M. Ceramic Trans. 2000;118:89.
[28] Molodov DA, Gottstein G, Prokofjev SI, Shvindlerman LS. In press.